Optical Clearing in the Kidney Reveals Potassium-Mediated Tubule Remodeling

Graphical Abstract

Highlights

- Tubule remodeling is assessable by immunolabeling optically cleared mouse kidneys

- A low-potassium diet leads to proliferation of various nephron segments

- Hyperplasia occurs in the proximal and distal tubules and medullary collecting duct

- Deletion of the renal potassium sensor Kir4.1 causes distal convoluted tubule atrophy

Authors

Turgay Saritas, Victor G. Puelles,
Xiao-Tong Su, James A. McCormick,
Paul A. Welling, David H. Ellison

Correspondence

tsaritas@ukaachen.de

In Brief

Saritas et al. use optical clearing, immunolabeling, and advanced light microscopy to assess potassium-mediated tubule remodeling in adult mouse kidneys. A low-potassium diet induced proliferation in specific tubule segments, including the distal convoluted tubule, and deletion of the renal potassium sensor Kir4.1 led to shortening of the distal convoluted tubule.
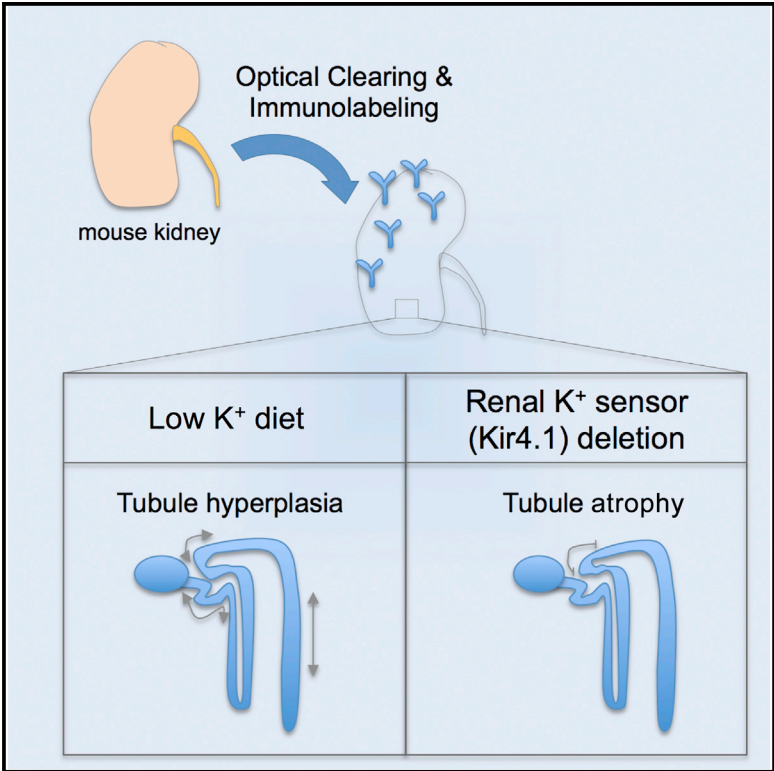
CellPress

Optical Clearing in the Kidney Reveals Potassium-Mediated Tubule Remodeling

Turgay Saritas,[1,2,8,*] Victor G. Puelles,[2,3,4] Xiao-Tong Su,[1] James A. McCormick,[1] Paul A. Welling,[5,6] and David H. Ellison[1,6,7]

[1]Division of Nephrology and Hypertension, Oregon Health & Science University, Portland, OR 97239, USA
[2]Division of Nephrology and Clinical Immunology, University Hospital RWTH Aachen, Aachen 52074, Germany
[3]III. Department of Medicine, University Medical Center, Hamburg-Eppendorf, Hamburg 20246, Germany
[4]Department of Nephrology, Monash Health, Melbourne, VIC 3168, Australia
[5]Department of Physiology, University of Maryland, Baltimore, MD 21201, USA
[6]Fondation LeDucq Transatlantic Networks of Excellence, Paris 75116, France
[7]Renal Section, Veterans Affairs Portland Health Care System, Portland, OR 97239, USA
[8]Lead Contact
*Correspondence: tsaritas@ukaachen.de
https://doi.org/10.1016/j.celrep.2018.11.021

SUMMARY

Distal nephron remodeling contributes to the pathophysiology of many clinically relevant scenarios, including diuretic resistance and certain Mendelian disorders of blood pressure. However, constitutive genetic disruptions are likely to have substantial developmental effects in this segment, and whether tubule remodeling upon physiological stimuli is a normal homeostatic mechanism is not known. Since the distal nephron acts as a potassium sensor, we assessed proliferation and tubule length in three dimensions upon dietary or inducible genetic manipulation by using optical clearing of adult mouse kidneys, whole-mount immunolabeling, and advanced light microscopy. We show that dietary potassium restriction leads promptly to proliferation of various nephron segments, including the distal convoluted tubule, whereas disruption of the potassium sensor Kir4.1 causes atrophy, despite ambient hypokalemia. These results provide proof that kidney tubules adapt rapidly to diet and indicate the power of clearing approaches to assess cell number and tubule length in healthy and diseased kidney.

INTRODUCTION

Renal epithelial cells contribute to tubule remodeling following kidney injury (Liu et al., 2017), long-term diuretic treatment (Kaissling et al., 1985), and genetic manipulation of tubule signaling pathways (Grimm et al., 2012, 2017). Tubule remodeling has been shown to associate with the production of autocrine and paracrine factors that may contribute to transport activation and hypertrophy, thereby protecting homeostasis (Grimm et al., 2015). Tubule hypertrophy, primarily of the collecting duct, has been reported during chronic hypokalemia (Elger et al., 1992), yet the recent recognition of a unique role for the distal convoluted tubule (DCT) in rapid potassium adaptation

(Terker et al., 2015; Welling, 2018) suggests that this nephron segment is especially sensitive. In line with this, molecular and anatomic changes are required for renal adaptation to occur following potassium stress, largely because dietary potassium deprivation leads to increased blood pressure (Terker et al., 2015). In the current model, hypokalemia is sensed by DCT cells via the basolateral potassium channel Kir4.1, thereby activating the thiazide-sensitive sodium-chloride cotransporter (NCC) and decreasing potassium secretion along more distal segments (Cuevas et al., 2017; Terker et al., 2015).

In humans, loss-of-function mutations in the gene encoding Kir4.1 cause seizures, sensorineural deafness, ataxia, mental retardation, and electrolyte imbalance (SeSAME) syndrome (OMIN: 612780) or epilepsy, ataxia, sensorineural deafness, and tubulopathy (EAST) syndrome (Bockenhauer et al., 2009), with a tubulopathy that mimics Gitelman syndrome (caused by NCC dysfunction) (OMIN: 263800); this tubulopathy is characterized by unrelenting potassium wasting and low blood pressure, testifying to the critical role of this nephron segment (Simon et al., 1996). These disease characteristics suggest that NCC abundance and functional activity are tightly coupled to that of Kir4.1 (Cuevas et al., 2017). Interestingly, it has been reported that constitutive NCC ablation causes DCT atrophy (Loffing et al., 2004), which likely contributes importantly to the clinical features of EAST or Gitelman syndromes. The hypothesis that activity along the DCT leads to morphological effects is supported by stereometric studies demonstrating that constitutive NCC activation increases the length of the DCT, whereas constitutive NCC inhibition shortens it (Grimm et al., 2012, 2017). However, these studies involved constitutive genetic manipulations that are likely to have substantial developmental effects. Additionally, observations regarding tubule remodeling in the DCT and other segments were made using two-dimensional techniques, which suffer from inherent biases. Here, we tested the hypothesis that short-term alterations in potassium balance lead to rapid tubule remodeling using two different models: dietary potassium deprivation and induced disruption of the DCT potassium sensor Kir4.1 (Cuevas et al., 2017). To address this question in an unbiased manner and thereby perform a more efficient and comprehensive analysis of tubule remodeling, we
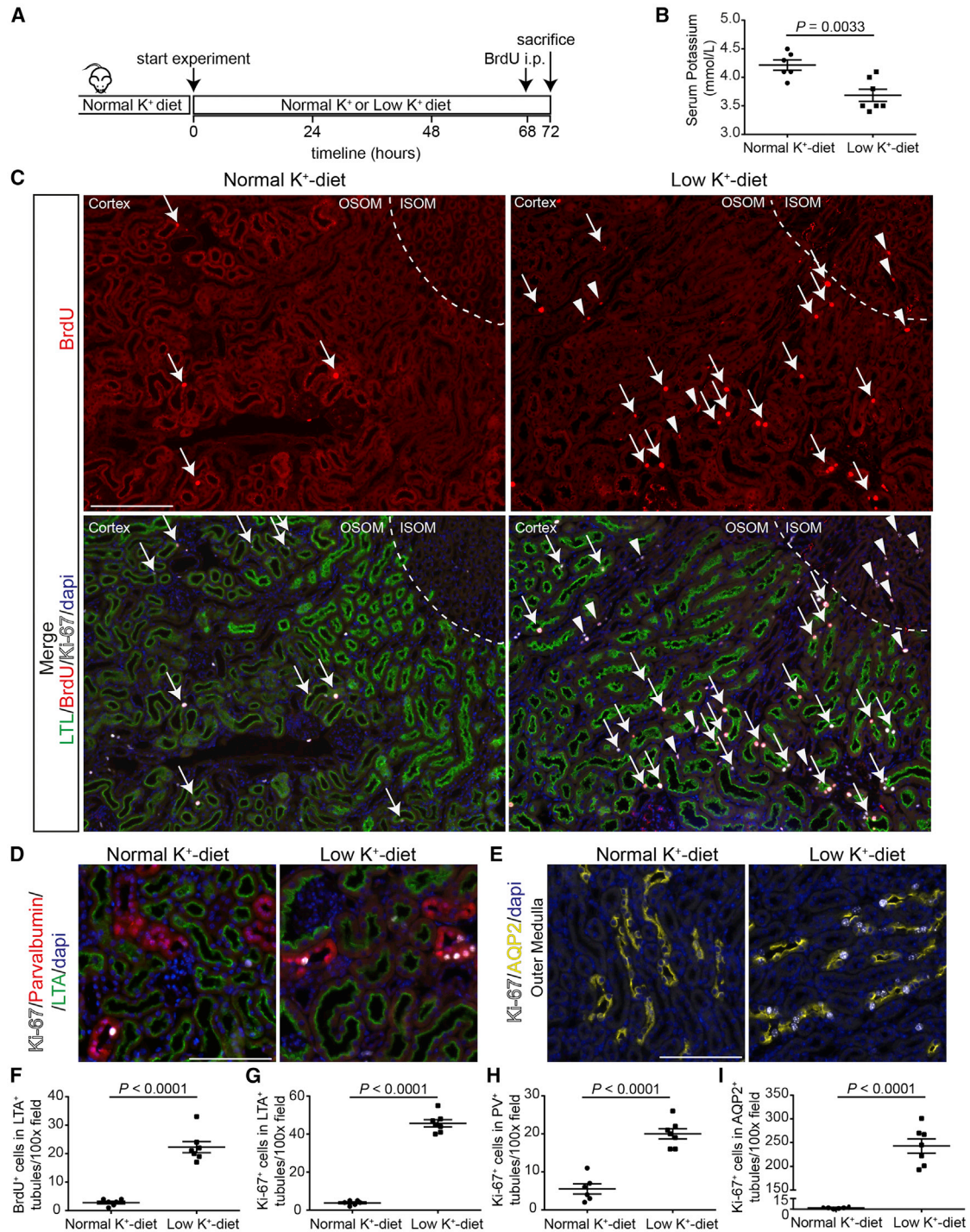
Figure 1. Effects of a 3-Day Low-Potassium Diet

(A) Adult C57BL/6J mice were fed for 3 days with a low-potassium diet or normal-potassium diet and then injected with bromodeoxyuridine (BrdU) intraperitoneally before kidneys were perfusion fixed 4 hr later.

(B) Blood potassium levels were lower in mice fed a low-potassium diet than in mice fed a normal-potassium diet.

(C) Immunofluorescence of 4-μm-thin sections revealed that a low-potassium diet increased the number of proliferating cells (BrdU [cells in S-phase] and Ki-67 [cells in G1, S, G2, or M-phase]) in the proximal tubule (LTL⁺, arrows) and other tubules or the peritubular space (arrowhead). Scale bar, 100 μm.

(D and E) A low-potassium diet induced a strong proliferative response in parvalbumin⁺ early distal convoluted tubule (DCT1) (D) and AQP2⁺ medullary collecting duct (E).

(legend continued on next page)

adapted whole-mount immunolabeling with highly validated and specific antibodies, optimized optical clearing methods, and advanced light microscopy for three-dimensional analysis of complete individual tubules. We focused on two main readouts of tubule remodeling (cell number and tubule length) and used two different optimized optical clearing methods (CLARITY and ethyl cinnamate [ECi]) (Chung et al., 2013; Klingberg et al., 2017). Here, we report determination of tubule remodeling in three dimensions by deep imaging of transparent mouse kidney slices and whole kidneys with confocal and light sheet microscopy.

RESULTS AND DISCUSSION

Tubule remodeling is an extremely dynamic process driven by constant physiological and morphological changes in the adult kidney. Most low-potassium diet studies have examined the long-term effects on kidney structure (Elger et al., 1992; Harada et al., 2005; Reungjui et al., 2008). Therefore, we restricted dietary potassium in wild-type mice for only 3 days and first used traditional two-dimensional techniques to analyze effects of diet on cell proliferation. A low-potassium diet reduced blood potassium levels compared to a normal-potassium diet (Figures 1A and 1B). Compared with mice on a normal potassium diet, mice on a low-potassium diet exhibited more proliferating cells as detected by bromodeoxyuridine (BrdU) labeling (which labels cells in S phase) and Ki-67 expression (which labels all proliferating cells); these were mainly localized in the proximal tubules (preferentially S3 segments; Figures 1C, 1F, and 1G), early parts of the DCT (DCT1; Figures 1D and 1H), and collecting ducts (preferentially in the medulla; Figures 1E and 1I). Additional proliferation in the peritubular space likely represents inflammatory cells (Figure 1C). Prolonged hypokalemia is known to cause hypokalemic nephropathy, characterized by tubule injury, hyperplasia of mainly medullary collecting ducts, interstitial macrophage infiltration, and tubulointerstitial fibrosis in animals and humans (Harada et al., 2005; Reungjui et al., 2008). No obvious proliferation was detected in other tubule segments (Figures S1 and S2). As summarized in Figures S1G and S2G, these data suggest segment-specific tubule remodeling after 3 days of dietary potassium restriction and extend previous findings with prolonged hypokalemia. Elger et al. (1992) demonstrated that kidney weight was 31% higher on an 18-day potassium-free diet and that hypertrophy was predominantly seen along the medullary collecting duct. Interestingly, endocycle-mediated hypertrophy, a phenomenon by which cells undergo DNA synthesis without cell division, has been recently uncovered in kidney tissue upon acute kidney injury (Lazzeri et al., 2018). Further studies are needed to determine the role of endocycles in kidney growth upon chronic potassium restriction. Our observation that a low-potassium diet caused cellular hyperplasia in the DCT suggests

that rapid tubule remodeling may be a normal homeostatic mechanism. The high incidence of proliferating cells found in the DCTs of mice on a low-potassium diet also supports the proposal that tubule remodeling is required to maintain homeostasis (Grimm et al., 2017).

After confirming that 3 days of a low-potassium diet was sufficient to induce proliferation in various nephron segments, we performed optical clearing of kidney tissue to assess the overall number of proliferating cells by determining the number of BrdU$^+$ cells (Figure 2A). In thick ethyl cinnamate-cleared kidney slices from control mice, cell proliferation was mainly restricted to the cortex (Figures 2B and 2D) and the outer stripe of the outer medulla (Figures 2C and 2E; Video S1). However, after 3 days on a low-potassium diet, the number of proliferating cells was increased in the cortex and more dramatically in the outer medulla (both the outer and inner stripe) (Figures 2B–2E). Because preferential hyperplasia occurred in medullary collecting duct cells, an antibody against aquaporin-2 (AQP2), a water channel specifically expressed in connecting tubules and collecting ducts, was used in both CLARITY- and ethyl cinnamate-cleared kidney slices (Figures 3A and 3B). We co-stained BrdU and AQP2 in ethyl cinnamate-cleared kidney slices to determine all BrdU$^+$ cells and those within the AQP2$^+$ tubules (Figure 3C; Video S2 and S3). In normal kidneys, ∼6% of all BrdU$^+$ cells were localized in medullary collecting ducts, whereas the proportion of proliferating cells in medullary collecting ducts from low-potassium-diet mice was higher (Figures 3C–3H). No signal was detected when kidneys were immersed in secondary antibody without previous incubation in primary antibody (Figures 3I and 3J). These results demonstrate that the combination of whole-mount immunolabeling, optical clearing, and advanced light microscopy allows for the performance of three-dimensional analysis of segment-specific tubule hyperplasia. This opens up many new areas of kidney research in both normal and diseased kidneys.

Using stereometric and other two-dimensional techniques, several studies in transgenic mice indicated that decreased NCC activity is associated with decreased DCT length and vice versa (Grimm et al., 2012, 2017; Lalioti et al., 2006; Loffing et al., 2004; McCormick et al., 2011). We observed that short-term dietary potassium restriction, which induces NCC activation via Kir4.1 (Cuevas et al., 2017; Terker et al., 2015), causes DCT cell proliferation. We hypothesized, therefore, that kidney-specific deletion of *Kir4.1* in adult mice, which we have shown decreases NCC activity by preventing DCT cells from sensing plasma [potassium], causes shortening of the DCT. By using pThr53-NCC antibody and propidium iodide (PI), we were able to detect DCTs and all nuclei in CLARITY-cleared kidneys (Figures 4A and 4B). We visualized and measured the length of entire DCTs, which exhibited substantial variability in lengths within the same kidney (Figures 4C and 4D; Video S4). As predicted, DCTs were

---

(F and G) Quantification of (C).

(H) Quantification of (D).

(I) Quantification of (E).

12 fields at 100× magnification were quantified from each sample.

Data are represented as mean ± SEM (n = 6–7 mice). p values were calculated using an unpaired two-tailed Student's t test. ISOM, inner stripe of the outer medulla; OSOM, outer stripe of the outer medulla; PV, parvalbumin.
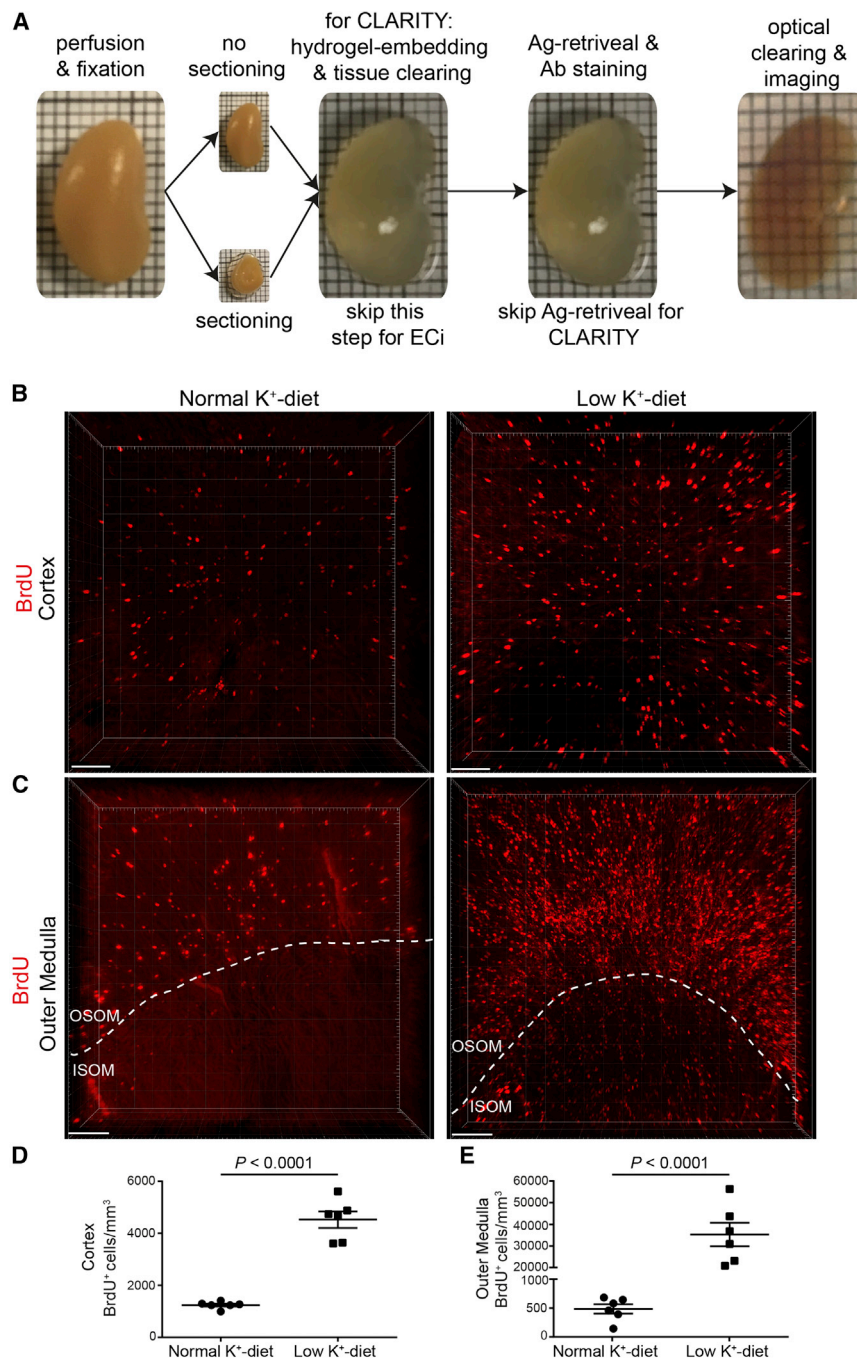
Figure 2. Optical Clearing and BrdU+ Cells in Ethyl-Cinnamate-Cleared Kidney Slices

(A) PFA-fixed kidneys were either sliced in thick slices or not sectioned, and then two different protocols were applied. For CLARITY, tissue was immersed in hydrogel monomer solution, polymerization was induced, and then tissue was cleared. For ethyl cinnamate (ECi), antigen retrieval was performed. In both protocols, tissue was then stained with antibodies or dye and optical clearing was performed using CLARITY (easy clear index solution) or ethyl cinnamate. Confocal and light sheet microscopy were used for volume imaging. Note that different kidneys are shown here.

(B and C) Three-dimensional visualization of a representative z stack shows an increased number of BrdU+ cells in the cortex (B) and outer medulla (C) in mice on a low-potassium diet compared to mice on a normal-potassium diet. ISOM, inner stripe of the outer medulla; OSOM, outer stripe of the outer medulla.

(D and E) Quantification of (B) and (C). Two kidney slices per sample were used, and from each kidney slice, five z stacks were taken from both the cortex (D) and outer medulla (E) (covering ~50% of the outer stripe [OSOM] and 50% of the inner stripe [ISOM]). Imaging was performed with confocal microscopy using a 10× objective lens (Zeiss LSM 880 with Airyscan).

Data are represented as mean ± SEM (n = 6 mice). p values were calculated using the unpaired two-tailed Student's t test. Scale bar, 100 μm. See also Video S1 (outer medulla under low potassium diet).

was used previously to estimate mouse DCT lengths from a three-dimensional reconstruction of 2,500 thick consecutive sections (Zhai et al., 2006). Here, we show that optical clearing combined with antibody labeling can be used to determine tubule length. In control mice, the length of the DCTs, using the accepted definition of segments that express NCC, was ~600 μm; this value is close to that estimated using the cumbersome and inferential reconstruction approach (Zhai et al., 2006). We also observed a significant shorting of the DCT after 5 weeks of *Kir4.1* deletion in adult mice, demonstrating that tubule remodeling is assessable with our approach.

significantly shorter in *Kir4.1* KO mice than in controls (Figure 4E), again, documenting tubule remodeling. No signal was detected when kidneys were immersed in secondary antibody without previous incubation in pThr53-NCC antibody (Figures 4F and 4G).

To date, the best method to estimate tubule length is stereology, which estimates the length of a tubule segment based on systemic sampling of the kidney (Nyengaard, 1999). This time-consuming procedure requires a high level of training and cannot visualize complete tubules (Puelles et al., 2017). This approach

We used two different optical clearing strategies, solvent based (ethyl cinnamate) and hydrogel embedded (CLARITY), and imaged with two different microscopes (confocal and light sheet). Since access to the light sheet is limited in many laboratories, we demonstrate that any laboratory with access to a confocal microscope can visualize and analyze intact kidney tubules. However, while confocal or two-photon microscopes give higher-resolution images and might be used preferentially to analyze tissue with single-cell resolution, their
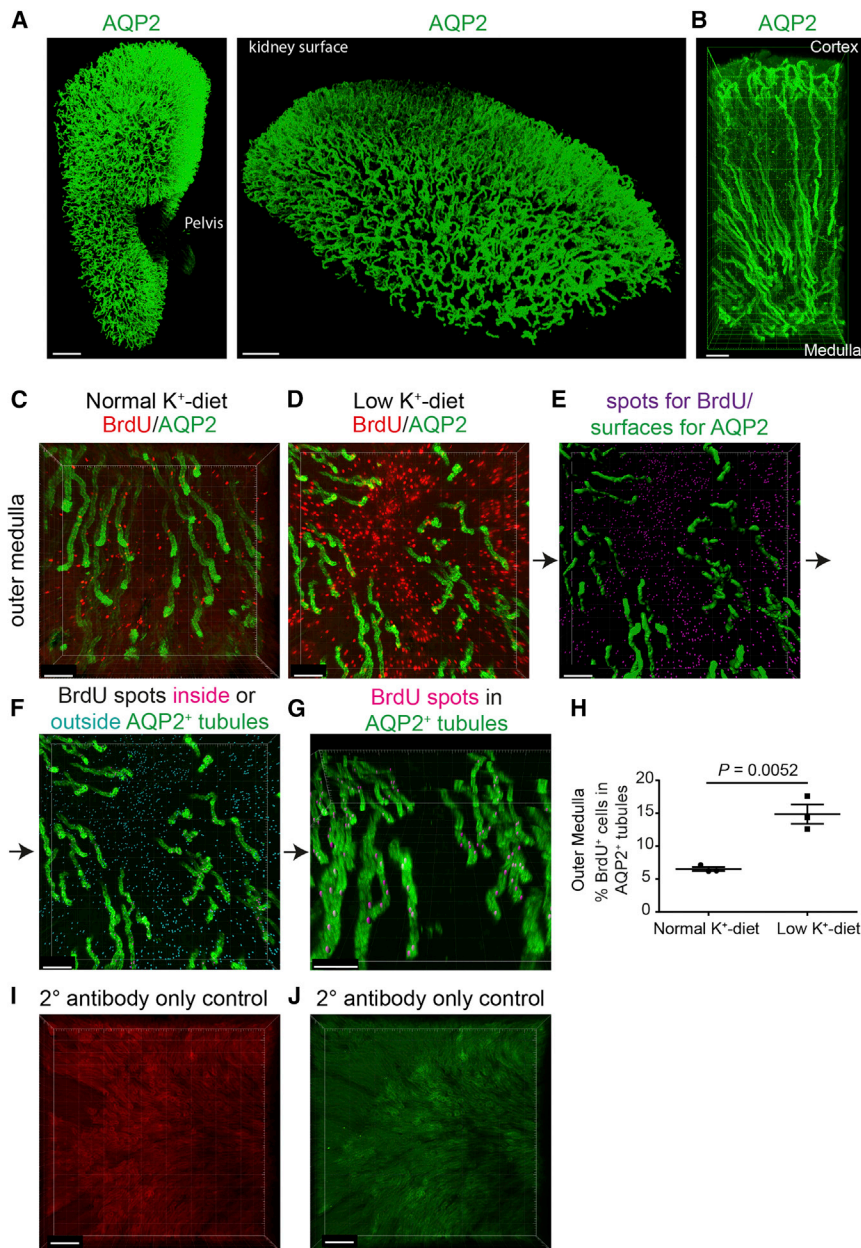
A AQP2   AQP2   kidney surface

Pelvis

B AQP2   Cortex   Medulla

C Normal K⁺-diet
BrdU/AQP2
outer medulla

D Low K⁺-diet
BrdU/AQP2

E spots for BrdU/
surfaces for AQP2

F BrdU spots inside or
outside AQP2⁺ tubules

G BrdU spots in
AQP2⁺ tubules

H

P = 0.0052

Outer Medulla
% BrdU⁺ cells in
AQP2⁺ tubules

Normal K⁺-diet   Low K⁺-diet

I 2° antibody only control   **J** 2° antibody only control

Figure 3. BrdU⁺ Cells in AQP2⁺ Tubules

(A) AQP2⁺ tubules in CLARITY-cleared control kidney. Scale bars, 1 mm.

(B) AQP2⁺ tubules in control kidney. The CLARITY protocol was first applied, and then tissue was washed, dehydrated, and cleared with ethyl cinnamate. Scale bar, 200 μm.

(C–D) Ethyl cinnamate-cleared kidney slices from mice on 3-day normal (C) or low (D) potassium diet were co-stained for AQP2 and BrdU.

(E–G) Data analysis process to determine BrdU⁺ cells within the AQP2⁺ medullary collecting duct in mice on low potassium diet.

(H) Quantification of BrdU⁺ cells within the AQP2⁺ medullary collecting duct in mice on normal (C) or low (D) normal and low-potassium diets. Two kidney slices per sample were used, and from each kidney slice, five z stacks were taken from the outer medulla (covering ~50% of the outer stripe [OSOM] and 50% of the inner stripe [ISOM]). Imaging was performed with confocal microscopy using a 10× objective lens (Zeiss LSM 880 with Airyscan). Data are represented as mean ± SEM (n = 3 mice). p values were calculated using an unpaired two-tailed Student's t test.

(I and J) A representative z stack shows an absence of nonspecific binding of secondary antibody (I, donkey anti-mouse Cy5 [pseudocolor: red]; J, donkey anti-goat Cy3 [pseudocolor: green]) without previous incubation in primary antibody. Scale bars, 100 μm.

Imaging was performed with a Zeiss Light Sheet Z1 using a 5× objective lens (A) and confocal microscopy using a 10× objective lens (B–G). See also Videos S2 and S3.

slow scanning speeds and limited penetration depth make them unrealistic for imaging large fields of view or whole organs. Light sheet microscopy is a superior option owing to its high imaging speed, reduced sample bleaching, and large fields of view (Tomer et al., 2014), which are required to visualize intact long tubule segments such as proximal tubules, thick ascending limbs, or collecting ducts. CLARITY and ethyl cinnamate are only two of the clearing approaches currently available, all of which have strengths and limitations in this rapidly growing field (Puelles et al., 2017). Most of these clearing approaches have been developed with a focus in neurobiology (Richardson and Lichtman, 2015), with only a few studies validating their application in other organs including the kidney (Klingberg et al., 2017; Puelles et al., 2016; Renier et al., 2014). CLARITY is ideal to visualize endogenous fluorescence of reporters such as GFP, which is partially quenched by solvent-based clearing (e.g., ethyl cinnamate) (Klingberg et al., 2017; Puelles et al., 2017). However, such reporters can also be visualized by antibody labeling, given the stability of fluorescent secondary antibodies and modified solvent-based protocols that preserve endogenous fluorescence signals (Masselink et al., 2018). In contrast to the original ethyl cinnamate protocol (Klingberg et al., 2017), our approach combines a modified ethyl cinnamate optical clearing method and immunolabeling, which uses an antigen-retrieval step to improve antibody binding. In the case of poor antibody penetration, however, the CLARITY protocol, which includes a lipid removal step, may be employed.

For quantitative analyses, we used sliced adult kidneys for several reasons. First, multiple questions can be addressed by staining kidney slices from one kidney with different antibodies. Second, the use of slices saves time and is more cost effective, because less time and antibody are needed to
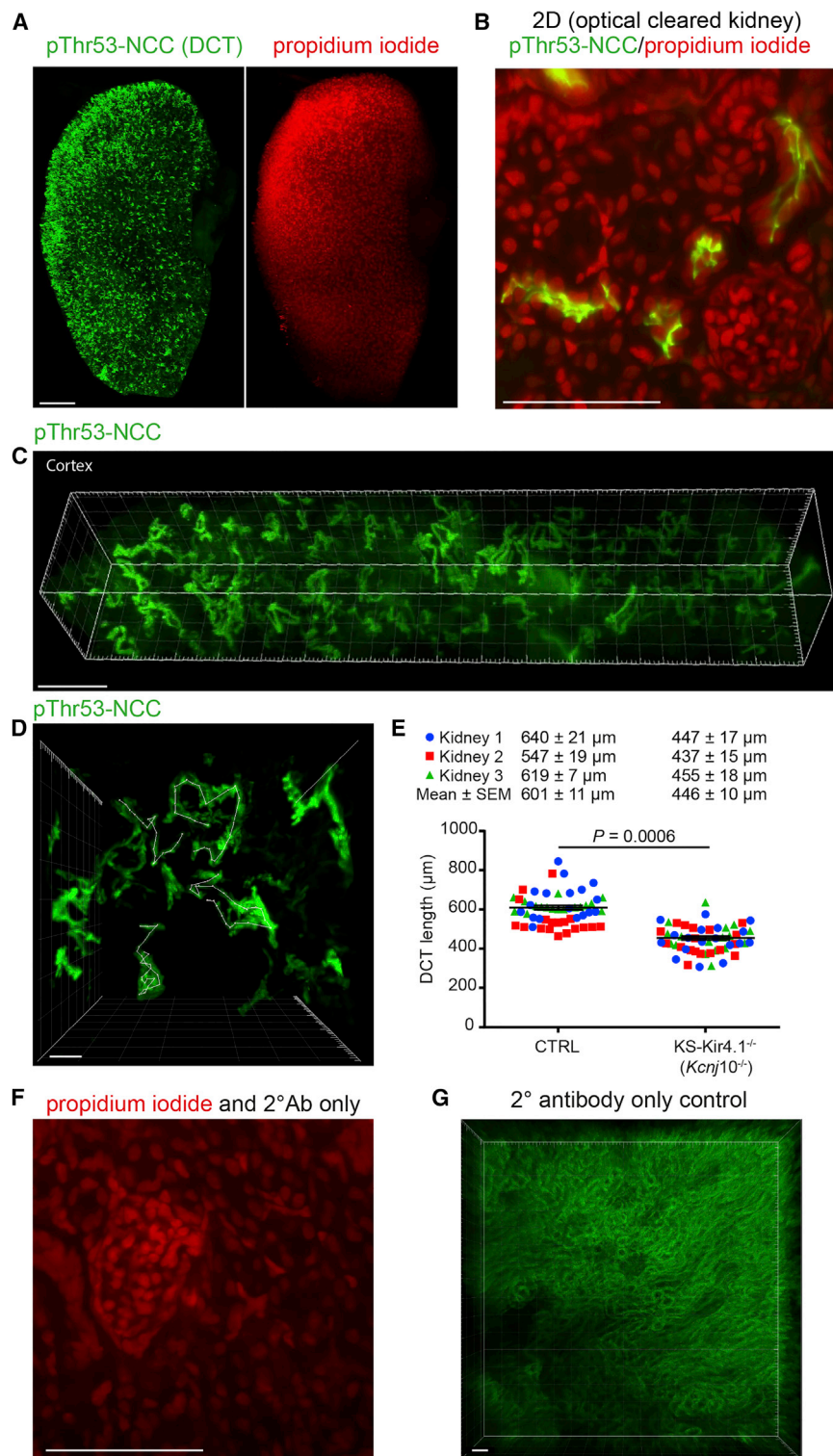
Figure 4. Quantification of DCT Length in Control and *Kir4.1* Knockout Mice

(A) Visualization of pThr53-NCC$^+$ DCTs and all nuclei using propidium iodide (PI) in whole optical cleared control kidney. Glomeruli are visible as bright red dots due to a higher density of PI$^+$ nuclei within glomeruli than surrounding tissue. Scale bar, 1 mm.

(B) One slice of a z stack showing apical staining of DCT and all nuclei using pThr53-NCC and PI. Scale bar, 100 μm.

(C) Low-magnification visualization of pThr53-NCC$^+$ DCTs. The z stack was taken along the cortical kidney surface. Scale bar, 300 μm.

(D) High-magnification visualization shows individual DCTs. The length was measured after three dimensional rendering using measurement points in Imaris software (white lines). Scale bar, 50 μm.

(E) Quantification of (D) shows that *Kir4.1* deletion is associated with a shortening of the DCT compared to controls (CTRL).

(F) One slice of a z stack showing all nuclei using PI and absence of nonspecific binding of secondary antibody (Ab) (donkey anti-rabbit Cy5) without previous incubation in pThr53-NCC antibody. Scale bar, 100 μm.

(G) No signal was detected in secondary antibody-only experiments (donkey anti-rabbit Cy5; pseudocolor: green) in ethyl cinnamate-cleared kidneys. Scale bar, 100 μm. 7–10 z stacks were taken with a 20× objective lens from the cortex of each kidney slice, and two kidney slices per animal were used.

Data are represented as mean ± SEM (n = 3 mice). p values were calculated using an unpaired two-tailed Student's t test. Imaging was performed with Zeiss Light Sheet Z1 using 5× (A) and 20× objective lenses (B–D and F). Zeiss LSM 880 confocal microscopy was used to take the image shown in (G). See also Video S4.

penetrate the tissue. Third, volume imaging generates large datasets (up to several terabytes), which makes it impossible for most workstations to perform complex algorithms such as automated counting, spot-to-surface measurements, or object tracing. Therefore, image stacks from smaller tissues or subsets of bigger files are more manageable to perform three dimensional (3D) analysis.

In conclusion, we demonstrate by a combination of whole-mount immunolabeling, optical clearing, advanced light microscopy, and three dimensional morphometric analysis that dietary potassium deprivation leads rapidly to tubule hyperplasia and an increase of proliferating cells in the tubulointerstitium. These specific changes occurred in various nephron segments, including the distal tubule, and might reflect an adaptive or maladaptive proliferative response upon potassium restriction, which is known to activate NCC and cause hypertension. In contrast, NCC inhibition by deletion of the potassium-sensor *Kir4.1* caused distal tubule atrophy. Use of this comprehensive tool allows reliable and efficient analysis of individual tubule

segments and is an ideal approach to better understand tubule remodeling.

STAR★METHODS

Detailed methods are provided in the online version of this paper and include the following:

- KEY RESOURCES TABLE
- CONTACT FOR REAGENT AND RESOURCE SHARING
- EXPERIMENTAL MODEL AND SUBJECT DETAILS
  - Mouse models
- METHOD DETAILS
  - Antibodies and chemicals
  - Low potassium diet
  - Blood biochemistry
  - Immunofluorescence of kidney sections
  - Optical clearing of the kidney
- QUANTIFICATION AND STATISTICAL ANALYSIS

SUPPLEMENTAL INFORMATION

Supplemental Information includes two figures and four videos and can be found with this article online at https://doi.org/10.1016/j.celrep.2018.11.021.

AUTHOR CONTRIBUTIONS

All authors designed the study, wrote the manuscript, and approved the final version of the manuscript. T.S., V.G.P., and X.-T.S. optimized the clearing protocols, performed the experiments, and conducted data analysis.

DECLARATION OF INTERESTS

The authors declare no competing interests.

REFERENCES

Bockenhauer, D., Feather, S., Stanescu, H.C., Bandulik, S., Zdebik, A.A., Reichold, M., Tobin, J., Lieberer, E., Sterner, C., Landoure, G., et al. (2009). Epilepsy, ataxia, sensorineural deafness, tubulopathy, and KCNJ10 mutations. N. Engl. J. Med. *360*, 1960–1970.

Chung, K., Wallace, J., Kim, S.Y., Kalyanasundaram, S., Andalman, A.S., Davidson, T.J., Mirzabekov, J.J., Zalocusky, K.A., Mattis, J., Denisin, A.K., et al.

(2013). Structural and molecular interrogation of intact biological systems. Nature *497*, 332–337.

Cuevas, C.A., Su, X.T., Wang, M.X., Terker, A.S., Lin, D.H., McCormick, J.A., Yang, C.L., Ellison, D.H., and Wang, W.H. (2017). Potassium sensing by renal distal tubules requires Kir4.1. J. Am. Soc. Nephrol. *28*, 1814–1825.

Elger, M., Bankir, L., and Kriz, W. (1992). Morphometric analysis of kidney hypertrophy in rats after chronic potassium depletion. Am. J. Physiol. *262*, F656–F667.

Grimm, P.R., Taneja, T.K., Liu, J., Coleman, R., Chen, Y.Y., Delpire, E., Wade, J.B., and Welling, P.A. (2012). SPAK isoforms and OSR1 regulate sodium-chloride co-transporters in a nephron-specific manner. J. Biol. Chem. *287*, 37673–37690.

Grimm, P.R., Lazo-Fernandez, Y., Delpire, E., Wall, S.M., Dorsey, S.G., Weinman, E.J., Coleman, R., Wade, J.B., and Welling, P.A. (2015). Integrated compensatory network is activated in the absence of NCC phosphorylation. J. Clin. Invest. *125*, 2136–2150.

Grimm, P.R., Coleman, R., Delpire, E., and Welling, P.A. (2017). Constitutively active SPAK causes hyperkalemia by activating NCC and remodeling distal tubules. J. Am. Soc. Nephrol. *28*, 2597–2606.

Harada, K., Akai, Y., Iwano, M., Nakatani, K., Nishino, T., Fujimoto, T., Shiiki, H., and Saito, Y. (2005). Tubulointerstitial macrophage infiltration in a patient with hypokalemic nephropathy and primary Sjögren's syndrome. Clin. Nephrol. *64*, 387–390.

Kaissling, B., Bachmann, S., and Kriz, W. (1985). Structural adaptation of the distal convoluted tubule to prolonged furosemide treatment. Am. J. Physiol. *248*, F374–F381.

Klingberg, A., Hasenberg, A., Ludwig-Portugall, I., Medyukhina, A., Männ, L., Brenzel, A., Engel, D.R., Figge, M.T., Kurts, C., and Gunzer, M. (2017). Fully automated evaluation of total glomerular number and capillary tuft size in nephritic kidneys using lightsheet microscopy. J. Am. Soc. Nephrol. *28*, 452–459.

Lalioti, M.D., Zhang, J., Volkman, H.M., Kahle, K.T., Hoffmann, K.E., Toka, H.R., Nelson-Williams, C., Ellison, D.H., Flavell, R., Booth, C.J., et al. (2006). Wnk4 controls blood pressure and potassium homeostasis via regulation of mass and activity of the distal convoluted tubule. Nat. Genet. *38*, 1124–1132.

Lazzeri, E., Angelotti, M.L., Peired, A., Conte, C., Marschner, J.A., Maggi, L., Mazzinghi, B., Lombardi, D., Melica, M.E., Nardi, S., et al. (2018). Endocycle-related tubular cell hypertrophy and progenitor proliferation recover renal function after acute kidney injury. Nat. Commun. *9*, 1344.

Liu, J., Kumar, S., Dolzhenko, E., Alvarado, G.F., Guo, J., Lu, C., Chen, Y., Li, M., Dessing, M.C., Parvez, R.K., et al. (2017). Molecular characterization of the transition from acute to chronic kidney injury following ischemia/reperfusion. JCI Insight *2*, 94716.

Loffing, J., Vallon, V., Loffing-Cueni, D., Aregger, F., Richter, K., Pietri, L., Bloch-Faure, M., Hoenderop, J.G., Shull, G.E., Meneton, P., and Kaissling, B. (2004). Altered renal distal tubule structure and renal Na(+) and Ca(2+) handling in a mouse model for Gitelman's syndrome. J. Am. Soc. Nephrol. *15*, 2276–2288.

Masselink, W., Reumann, D., Murawala, P., Pasierbek, P., Taniguchi, Y., Knoblich, J.A., and Tanaka, E.M. (2018). Broad applicability of a streamlined ethyl cinnamate-based clearing procedure. bioRxiv. https://doi.org/10.1101/346247.

McCormick, J.A., Mutig, K., Nelson, J.H., Saritas, T., Hoorn, E.J., Yang, C.L., Rogers, S., Curry, J., Delpire, E., Bachmann, S., and Ellison, D.H. (2011). A SPAK isoform switch modulates renal salt transport and blood pressure. Cell Metab. *14*, 352–364.

Mutig, K., Saritas, T., Uchida, S., Kahl, T., Borowski, T., Paliege, A., Böhlick, A., Bleich, M., Shan, Q., and Bachmann, S. (2010). Short-term stimulation of the thiazide-sensitive Na+-Cl- cotransporter by vasopressin involves phosphorylation and membrane translocation. Am. J. Physiol. Renal Physiol. *298*, F502–F509.

Nyengaard, J.R. (1999). Stereologic methods and their application in kidney research. J. Am. Soc. Nephrol. *10*, 1100–1123.

Puelles, V.G., van der Wolde, J.W., Schulze, K.E., Short, K.M., Wong, M.N., Bensley, J.G., Cullen-McEwen, L.A., Caruana, G., Hokke, S.N., Li, J., et al. (2016). Validation of a three-dimensional method for counting and sizing podocytes in whole glomeruli. J. Am. Soc. Nephrol. 27, 3093–3104.

Puelles, V.G., Moeller, M.J., and Bertram, J.F. (2017). We can see clearly now: optical clearing and kidney morphometrics. Curr. Opin. Nephrol. Hypertens. 26, 179–186.

Renier, N., Wu, Z., Simon, D.J., Yang, J., Ariel, P., and Tessier-Lavigne, M. (2014). iDISCO: a simple, rapid method to immunolabel large tissue samples for volume imaging. Cell 159, 896–910.

Reungjui, S., Roncal, C.A., Sato, W., Glushakova, O.Y., Croker, B.P., Suga, S., Ouyang, X., Tungsanga, K., Nakagawa, T., Johnson, R.J., and Mu, W. (2008). Hypokalemic nephropathy is associated with impaired angiogenesis. J. Am. Soc. Nephrol. 19, 125–134.

Richardson, D.S., and Lichtman, J.W. (2015). Clarifying tissue clearing. Cell 162, 246–257.

Saritas, T., Borschewski, A., McCormick, J.A., Paliege, A., Dathe, C., Uchida, S., Terker, A., Himmerkus, N., Bleich, M., Demaretz, S., et al. (2013). SPAK differentially mediates vasopressin effects on sodium cotransporters. J. Am. Soc. Nephrol. 24, 407–418.

Simon, D.B., Nelson-Williams, C., Bia, M.J., Ellison, D., Karet, F.E., Molina, A.M., Vaara, I., Iwata, F., Cushner, H.M., Koolen, M., et al. (1996). Gitelman's variant of Bartter's syndrome, inherited hypokalaemic alkalosis, is caused by mutations in the thiazide-sensitive Na-Cl cotransporter. Nat. Genet. 12, 24–30.

Smeets, B., Boor, P., Dijkman, H., Sharma, S.V., Jirak, P., Mooren, F., Berger, K., Bornemann, J., Gelman, I.H., Floege, J., et al. (2013). Proximal tubular cells contain a phenotypically distinct, scattered cell population involved in tubular regeneration. J. Pathol. 229, 645–659.

Terker, A.S., Zhang, C., McCormick, J.A., Lazelle, R.A., Zhang, C., Meermeier, N.P., Siler, D.A., Park, H.J., Fu, Y., Cohen, D.M., et al. (2015). Potassium modulates electrolyte balance and blood pressure through effects on distal cell voltage and chloride. Cell Metab. 21, 39–50.

Tomer, R., Ye, L., Hsueh, B., and Deisseroth, K. (2014). Advanced CLARITY for rapid and high-resolution imaging of intact tissues. Nat. Protoc. 9, 1682–1697.

Traykova-Brauch, M., Schönig, K., Greiner, O., Miloud, T., Jauch, A., Bode, M., Felsher, D.W., Glick, A.B., Kwiatkowski, D.J., Bujard, H., et al. (2008). An efficient and versatile system for acute and chronic modulation of renal tubular function in transgenic mice. Nat. Med. 14, 979–984.

Wall, S.M., and Lazo-Fernandez, Y. (2015). The role of pendrin in renal physiology. Annu. Rev. Physiol. 77, 363–378.

Welling, P.A. (2018). WNKs on the fly. J. Am. Soc. Nephrol. 29, 1347–1349.

Zhai, X.Y., Thomsen, J.S., Birn, H., Kristoffersen, I.B., Andreasen, A., and Christensen, E.I. (2006). Three-dimensional reconstruction of the mouse nephron. J. Am. Soc. Nephrol. 17, 77–88.

STAR★METHODS

KEY RESOURCES TABLE

REAGENT or RESOURCE	SOURCE	IDENTIFIER
Antibodies		
Anti-BrdU monoclonal antibody	Roche	Cat#11296736001
Rabbit anti-Ki-67	Vector Laboratories	Cat#VP-RM04; RRID: AB_2336545
Goat anti-AQP2	Santa Cruz Biotechnology	Cat#sc-9882; RRID: AB_2289903
Rabbit anti-phoshoThr53-NCC	PhosphoSolutions	Cat#p1311-53; RRID:AB_2650477
Guinea pig anti-NKCC2	Saritas et al., 2013	N/A
Rabbit anti-pT96/T101-NKCC2	Saritas et al., 2013	N/A
Guinea pig anti-pendrin	Wall and Lazo-Fernandez, 2015	N/A
Guinea pig anti-parvalbumin	Swant	Cat#GP72; RRID: AB_2665495 RRID:AB_2665495
Mouse anti-calbindin D-28k	Swant	Cat#300; RRID: AB_10000347
Donkey anti–goat Cy3	Life Technologies	Cat#A21432; RRID:AB_141788
Donkey anti–mouse Cy5	Life Technologies	Cat#A31571; RRID: AB_162542
Donkey anti–rabbit Cy5	Life Technologies	Cat#A31573; RRID: AB_2536183
Chemicals		
Fluorescein labeled Lotus Tetragonolobus Lectin	Vectorlabs	Cat#FL-1321; RRID: AB_2336559
Propidium iodide	Life Technologies	Cat#P3566
Doxycycline	Alfa Aesar	Cat#J60579
Citrate-based antigen retrieval solution	Vector Laboratories	Cat#H-3300; RRID:AB_2336226
DAPI mounting medium	Thermo Fischer Scientific	Cat#P36971
Envision Flex Wash Buffer	Agilent	Cat#K800721-2
Antibody diluent	Dako	Cat#S0809
Ethanol	Merck	Cat#100983
Ethyl cinnamate	Sigma-Aldrich	Cat#112372
Acrylamide	Bio-Rad	Cat#161-0140
Azo initiator	Wako	Cat#VA-044
Paraformaldehyde	Thermo Fischer Scientific	Cat#O4042-500
Easy Index clearing solution	Lifecanvas Technologies	Cat#EI-Z1001
Experimental Models: Organisms/Strains		
Mouse: Pax8-rtTA/LC-Kcnj10fl/fl	Cuevas et al., 2017	N/A
Mouse: C57BL/6J	The Jackson Laboratory	Stock No: 000664
Software and Algorithms		
Imaris	http://www.bitplane.com/imaris/imaris	N/A
Arivis 4D	https://www.arivis.com/en/imaging-science/arivis-vision4d	N/A
GraphPad Prism	https://www.graphpad.com/scientific-software/prism/	N/A
Other		
Potassium-deficient diet	Envigo	Cat#TD.88239
Normal potassium diet	Labdiet	Cat#5LOD

CONTACT FOR REAGENT AND RESOURCE SHARING

Further information and requests for resources and reagents should be directed to and will be fulfilled by the Lead Contact, Turgay Saritas (tsaritas@ukaachen.de).

EXPERIMENTAL MODEL AND SUBJECT DETAILS

Mouse models

Studies were approved by Oregon Health and Science University's Animal Care and Use Committee (Protocol IP00286). For the low potassium diet study, male and female C57BL/6 mice were used between 12–24 weeks of age (average weight: 25–30 g). All strains are backcrossed to the appropriate wild-type mice every ten generations to maintain genetic backgrounds. For the measurement of the distal convoluted tubule length, kidney-specific *Kcnj10* deletion was carried out in 8 to 12-week-old mice homozygous for the floxed *Kcnj10* gene (Cuevas et al., 2017) and hemizygous for the Pax8-rtTA/LC-1-Cre transgene (Traykova-Brauch et al., 2008) by providing doxycycline (2 mg/ml; Alfa Aesar, Cat#J60579) in 5% sucrose/drinking water for 3 weeks. This was followed by at least 2 additional weeks of washout period, before performing experiments. Littermate mice of the same age and genetic background were given 5% sucrose via drinking water and were used as controls (*Kcnj10*$^{fl/fl}$). The complete procedure and genotyping were previously reported (Cuevas et al., 2017). All mice were bred in-house and were group housed (up to 5 mice per cage).

METHOD DETAILS

Antibodies and chemicals

A list of antibodies and chemicals including vendor and catalog numbers is provided in Key Resources Table.

Low potassium diet

For quantification of BrdU$^+$ cells following normal or low potassium diet, mice were fed for 3 days with potassium-deficient diet (approx. 0.002% potassium; Envigo, Cat#TD.88239) or normal potassium diet (1.2% potassium, Labdiet, Cat#5LOD) and were injected with BrdU (40 mg/kg b.w.; Roche, Cat#11296736001) intraperitoneally before kidneys were perfusion-fixed 4 h later. Water was provided *ad libitum*.

Blood biochemistry

Blood was collected via cardiac puncture under isoflurane anesthesia and transferred into heparinized tubes; 80 μL was immediately loaded into a Chem8+ cartridge for electrolyte measurement in an i-STAT analyzer (Abbot Point of Care Inc., Princeton, NJ, USA).

Immunofluorescence of kidney sections

Kidneys were fixed by retrograde abdominal aortic perfusion of 3% paraformaldehyde and embedded in paraffin. Four micrometer sections were dewaxed and rehydrated by successive immersion for 5 min in 100% xylene, 100%, 90% and 70% ethanol solutions. Following heat-induced citrate-based antigen retrieval (Vector Laboratories, Cat#H-3300), immunostaining was performed using the following primary antibodies in 1% BSA/PBS (BrdU, Roche, Cat#11296736001; Ki-67, Vector Laboratories, Cat#VP-RM04; AQP2, Santa Cruz Biotechnology, Cat#sc-9882; pThr53-NCC (generated in laboratory of D.H.E; commercially available from Phosphoso-lution, Cat#p1311-53 (McCormick et al., 2011; Mutig et al., 2010)); total Na$^+$-potassium-2Cl$^-$ (NKCC2) and pT96/T101-NKCC2 (gift from Sebastian Bachmann, (Saritas et al., 2013)); Pendrin (gift from Susan Wall, (Wall and Lazo-Fernandez, 2015)). Fluorescein-labeled Lotus Tetragonolobus Lectin (LTL-FITC; Vectorlabs, Cat#FL-1321) was used to identify proximal tubules (Smeets et al., 2013). Cy2-, Cy3-, or Cy5-conjugated antibodies (Thermo Fisher Scientific) served as secondary antibodies and 4',6-Diamidino-2-phenylindole-containing mounting medium (Thermo Fisher Scientific, Cat#P36971) was used for nuclear staining. 12 images from each kidney section were captured at 100X magnification on a Carl Zeiss AxioImager.M2 using AxioVision SE64 software.

Optical clearing of the kidney

PFA perfusion-fixed kidneys, cut into either 1-2 mm thick kidney slices or kept whole (Figure 2A), were post-fixed in PFA for at least 3 days at room temperature, then washed in 1X wash buffer (Agilent, Envision Flex Wash Buffer, Cat#K800721-2) and placed on a horizontal shaker overnight at room temperature. Then, one of the two following kidney-optimized protocols was used:

Ethyl cinnamate

We applied our recently published immunoflourescence protocol on thick kidney slices (Puelles et al., 2016). Antigen retrieval was performed using antigen retrieval solution (Vector Laboratories, Cat#H-3300) for 1 hour at 92-98°C then the slices were left to cool. After a wash in wash buffer overnight at room temperature, slices were immersed in 500 μL primary antibody solution made up in antibody diluent (Dako, Cat#S0809) using BrdU (1:100; Roche, Cat#11296736001) and/or AQP2 (1:150; Santa Cruz Biotechnology, Cat#sc-9882) at 37°C for 4 days. Slices were then washed in wash buffer for 24 hours with one change of wash buffer after 8 hours. Next, slices were immersed in 500 μL secondary antibody solution made up in antibody diluent using a donkey anti–goat Cy3 (to detect AQP2) (1:200; Life Technologies, Cat#A21432) and a donkey anti–mouse Cy5 (to detect Brdu) (1:200; Life Technologies, Cat#A31571). Slices were washed again in wash buffer on an orbital shaker for 24 hours with one change of wash buffer after 8 hours, then placed in high grade 100% ethanol (Merck; Cat#100983) for 1hr at room temperature with gentle shaking (with at least one change to fresh ethanol). They were directly immersed in ethyl cinnamate (Sigma-Aldrich; Cat#112372) and gently agitated overnight at room temperature under light protection. Tissue translucency was achieved in less than 1hr. In contrast to Klingberg et al. (Klingberg et al., 2017), we did not immerse kidney slices in sequential ascending ethanol dilutions, which saved time and increased efficiency.

CLARITY

We modified a previously published protocol by Chung et al. (Chung et al., 2013). Kidney slices or whole kidney were immersed in hydrogel monomer solution (4% acrylamide (Bio-Rad, Cat#161-0140), 0.25% Azo initiator (Wako, Cat#VA-044), 1X PBS, and 4% PFA (Thermo Fischer Scientific, Cat#O4042-500) in UltraPure water) at 4°C for 3 or 7 days, respectively. Hydrogel polymerization was induced under argon atmosphere (O_2 free) at 37°C for 3hrs. Samples were washed with 1x wash buffer overnight at room temperature, then placed in Smart Clear II Pro (Lifecanvas Technologies) for 3 days (kidney slices) or 7 days (whole kidney). Samples were washed with 1x wash buffer overnight at room temperature, then immunofluorescence protocol was performed as described in the ethyl cinnamate section with the exception that we did not perform antigen retrieval, and tissue was stained with pThr53-NCC (1:100) or propidium iodide (PI, 1:1000, Life Technologies, Cat#P3566). pThr53-NCC-stained samples were washed overnight and then incubated with donkey anti–rabbit Cy5 (1:200; Life Technologies, Cat#A31573) for 4 days. Imaging was performed after at least 24hrs of incubation in Easy Index clearing solution (Lifecanvas Technologies, Cat#EI-Z1001).

For ethyl cinnamate-cleared samples we used a confocal microscope (Zeiss LSM 880 with Airyscan, 10x objective lens). From each kidney slice, five z stacks were taken from both cortex and outer medulla (approximately covering 50% outer stripe (OSOM), 50% inner stripe (ISOM)). For each experiment, two kidney slices per animal were used. Fluorescence signal was generated by excitiation at 555nm and 647nm using a DPSS 561 and a HeNE laser. For imaging of CLARITY-cleared samples, we used a light sheet microscope (Zeiss Z1, 5x and 20x CLARITY-optimized objective lenses). 7-10 z stacks were taken from cortex of each kidney slice, and two kidney slices per animal were used. For both microscopes Zen software (Carl Zeiss) was used.

QUANTIFICATION AND STATISTICAL ANALYSIS

For quantification of the number of BrdU[+] or Ki-67^{+} cells on thin kidney sections, 12 images (100x field) were randomly taken per cortex and outer medulla. The number of cells was counted using ImageJ and expressed as number of cells per field.

For quantification of sample volume, BrdU^{+} cells (spots) and DCT length (length of connected measurement points) were performed using three dimensional rendering and analysis software (Imaris, v9.2.1; Bitplane, AG). The following criteria were set for the analysis of BrdU spots: size 8 μm in xy-axis, 14 μm in z axis (values were determined by measuring diameter in xy axis in 2D/slice view, and length in z axis using three dimensional view). DCTs touching the boundary of the section were excluded since they could represent incomplete tubules. Three dimensional rendering of PI[+] nuclei, AQP2^{+} and pThr53-NCC[+] tubules was performed using Arivis Vision4D (Arivis AG). Statistical parameters including the exact value of n, the definition of center, dispersion and precision measures (mean ± SEM) and statistical significance are reported in the Figures and Figure Legends. Data was judged to be statistically significant when $p < 0.05$ by parametric unpaired two-tailed Student's t test. Statistical analysis was performed in GraphPad PRISM 6 (GraphPad software Inc., La Jolla, CA).

Supplemental Information

Optical Clearing in the Kidney Reveals

Potassium-Mediated Tubule Remodeling

Turgay Saritas, Victor G. Puelles, Xiao-Tong Su, James A. McCormick, Paul A. Welling, and David H. Ellison

Inventory of Supplemental Information

Figure S1. Related to Figure 1. Segment-specific localization of Ki-67$^+$ cells in thin kidney sections.

Figure S2. Related to Figure 1. Segment-specific localization of BrdU$^+$ cells in thin kidney sections.
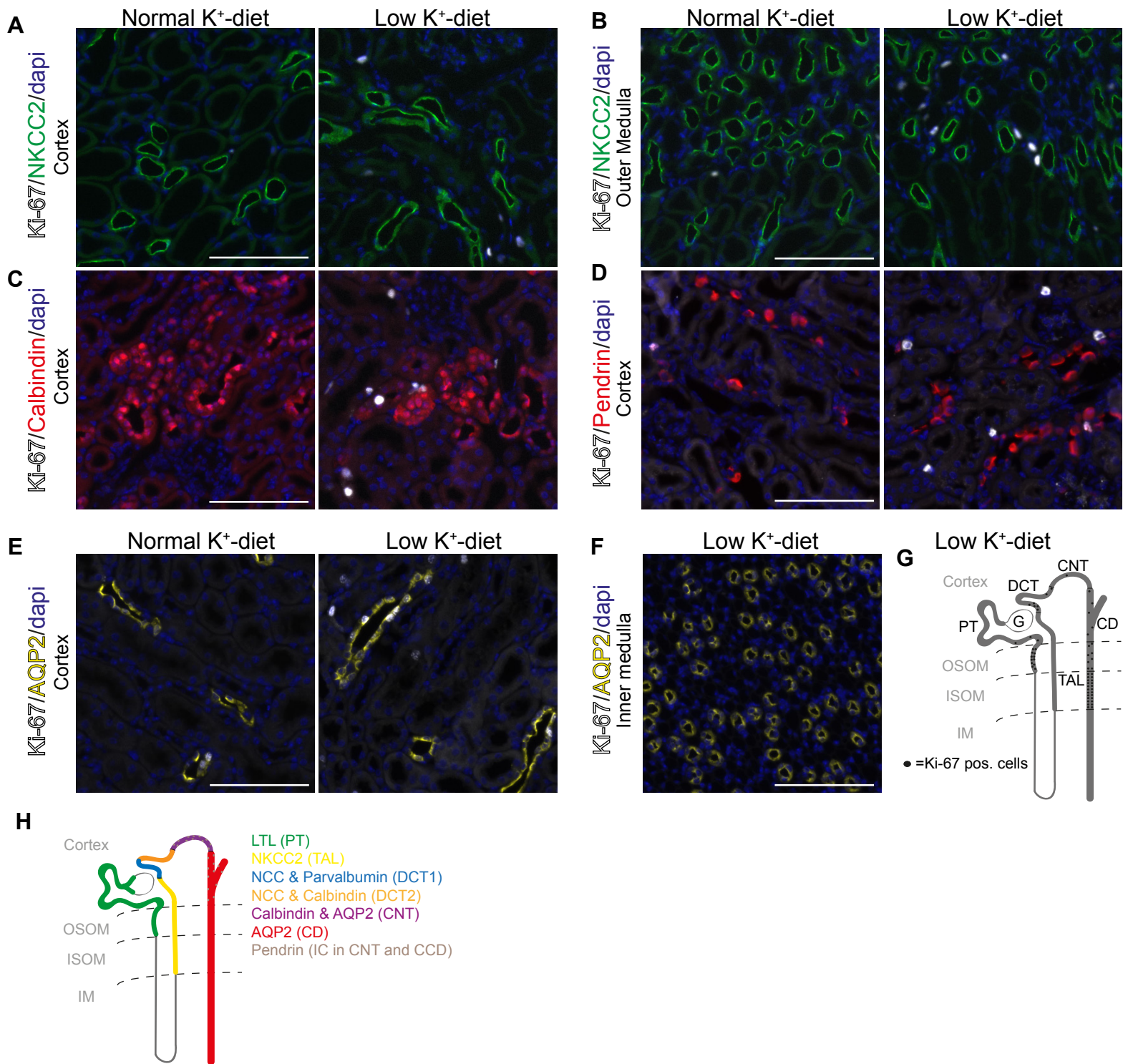
Figure S1. Related to Figure 1. Segment-specific localization of Ki-67+ cells in thin kidney sections. A-D: No or only few Ki-67+ cells were found in cortical or medullary NKCC2+ thick ascending limb of henle (TAL), calbindin+ distal convoluted tubule (DCT2)/connecting tubule (CNT) or pendrin+ intercalated cells (IC). **E, F:** Ki-67+ cells were observed in AQP2+ cortical collecting duct (CCD), but not in inner medulla. **G:** Summary of low K+-induced segment-specific proliferation based on Ki-67 immunolabeling. **H:** Scheme of the investigated tubule segments: Lotus Tetragonolobus Lectin (LTL) was used to label brush borders specific for proximal tubules (PT). PT reabsorbs salt, water and organic solutes and secretes ammonium into the lumen. Antibody against sodium-potassium-chloride-contransporter 2 (NKCC2) was used to label TAL, which is relevant for salt reabsorption. Sodium-Chloride-cotransporter (NCC) is specifically expressed in entire DCT, whereas parvalbumin and calbindin are expressed in DCT1 and DCT2, respectively. DCT1 and 2 play a differential role in ion transport. Calbindin is also expressed in CNT. Pendrin is expressed in IC in CNT and CCD, where it is involved in bicarbonate secretion. Aquaporin-2 (AQP2) is expressed in CNT and collecting duct (CD), and both segments are involved in urine concentration and electrolyte transport. *n* = 6-7 mice.

Figure S2. Related to Figure 1. Segment-specific localization of BrdU+ cells. A: Immunofluorescence of 4 µm thin sections revealed that low K+ diet increased number of BrdU+ cells in inner stripe of the outer medulla (ISOM). **B:** Arrows indicate BrdU+ cell in proximal tubules (LTL+) and medullary collecting duct (AQP2+). **C-F:** Low-K+ diet induced proliferation in DCT1 (parvalbumin+, pNCC+) (D), but not in thick ascending limb (NKCC2+) (C), DCT2 (calbindin+, pNCC+) (E), connecting tubules (calbindin+) (E) or intercalated cells in the distal nephron (pendrin+) (F). **G:** Summary of low K+-induced segment-specific proliferation based on BrdU immunolabeling. All scale bars = 100 µm. *n* = 6-7 mice. OSOM, outer stripe of the outer medulla; IM, inner medulla.